

Cross sections, multiplicity and moment distributions at the LHC

P.C. Beggio^{1,2} and E.G.S. Luna²

¹*Laboratório de Ciências Matemáticas,*

Universidade Estadual do Norte Fluminense Darcy Ribeiro,

28013-602, Campos dos Goytacazes, RJ, Brazil

²*Instituto de Física, Universidade Federal do Rio Grande do Sul,*

CP 15051, 91501-970, Porto Alegre, RS, Brazil

Abstract

The unitarity of the S -matrix requires that the absorptive part of the elastic scattering amplitude receives contributions from both the inelastic and the elastic channels. We explore this unitarity condition in order to describe, in a connected way, hadron-hadron observables like the total and elastic differential cross sections, the ratio of the real to imaginary part of the forward scattering amplitude and the inclusive multiplicity distributions in full phase space, over a large range of energies. We introduce non-perturbative QCD effects in the forward scattering amplitude by using the infrared QCD effective charge dependent on the dynamical gluon mass. In our analysis we pay special attention to the theoretical uncertainties in the predictions due to this mass scale variation. We also present quantitative predictions for the H_q moments at high energies. Our results reproduce the moment oscillations observed in experimental data, and are consistent with the behavior predicted by QCD.

I. INTRODUCTION

The study of multiple production of particles at high energies has been a subject of intense theoretical and experimental interest. Its importance lies in the fact that the multiplicity distributions of charged hadrons provide central information on the mechanism of production of the particles [1–4]. Existing models for particle production are usually based on QCD since the production of hadrons can, at the microscopic level, be associated with the copious creation of color partons through gluon radiation. However, this approach also contains a phenomenological component as the hadronization, the transition of the quark-gluon system to hadrons, involves a soft scale, and therefore purely perturbative techniques do not apply [1–3, 5, 6].

The non-perturbative character of the QCD is also manifest in the elastic channel since at high energies the soft and the semihard components of the scattering amplitude are closely related [7]. Thus, in considering the forward scattering amplitude for elastic hadron-hadron collisions, it becomes important to distinguish between semihard gluons, which participate in hard parton-parton scattering, and soft gluons, emitted in any given parton-parton QCD radiation process.

Fortunately, our task of describing hadron-hadron observables in both elastic and inelastic channels, bringing up information about the infrared properties of QCD, can be properly addressed by considering the possibility that the non-perturbative dynamics of QCD generate an effective gluon mass. This dynamical gluon mass is intrinsically related to an infrared finite strong coupling constant, and its existence is strongly supported by recent QCD lattice simulations [8] as well as by phenomenological results [9–12]. More specifically, a global description of elastic and inelastic hadronic observables can succeed in a consistent way by introducing a non-perturbative QCD effective charge in the calculation of the gluon-gluon total cross section, which dominates at high energy and determines the asymptotic behavior of hadron-hadron cross sections, and by exploring the unitarity condition of the S -matrix in impact parameter space, which relates the elastic scattering amplitudes to the inelastic overlap function G_{in} .

With this background in mind, the main purpose of this paper is to explore the non-perturbative dynamics of QCD in order to describe in a connected way hadron-hadron observables in both elastic and inelastic channels, assuming the eikonal representation and

the unitarity condition of the scattering matrix, and compare the results with the pp and $\bar{p}p$ experimental data of total and elastic differential cross sections, the parameter ρ and the inclusive multiplicity distributions in full phase space.

The paper is organized as follows: in the next section we introduce a QCD-based eikonal model where the onset of the dominance of semihard gluons in the interaction of high-energy hadrons is managed by the dynamical gluon mass. Motivated by the recent TOTEM measurement of the pp total cross section, σ_{tot}^{pp} , at LHC, we perform a detailed analysis of pp and $\bar{p}p$ forward scattering data and elastic differential cross sections using our eikonal model, and obtain predictions for $\sigma_{tot}^{pp,\bar{p}p}$, $\rho^{pp,\bar{p}p}$ and $d\sigma^{\bar{p}p}/dt$ at Tevatron and CERN-LHC energies. We evaluate the theoretical uncertainty associated with the dynamical mass scale and obtain predictions with uncertainty bands for $\sigma_{tot}^{pp,\bar{p}p}$ and $\rho^{pp,\bar{p}p}$. In Sec. III we present the basic formalism, as well as the underlying physical picture, of multiplicity distributions associated with charged hadron production, and introduce the theoretical prescription for connecting the elastic and inelastic channels. With the parameters of the eikonal fixed from the elastic fit, we calculate the multiplicity distribution P_n in pp and $\bar{p}p$ collisions over a large range of energies, and study the effect of the mass scale uncertainty on high multiplicities. In the sequence we calculate the H_q moments of the multiplicity distributions at high energies, where we observe that our results reproduce the oscillatory behavior predict by QCD. In Sec. IV we draw our conclusions.

II. ELASTIC CHANNEL: THE DYNAMICAL GLUON MASS MODEL

QCD-inspired models are at present one of the main theoretical approaches to explain the observed increase of hadron-hadron total cross sections [10, 11, 13]. These models incorporate soft and semihard processes in the treatment of high-energy hadron-hadron interactions using a formulation compatible with analyticity and unitarity constraints. In the eikonal representation the total and inelastic cross sections are given by

$$\sigma_{tot}(s) = 4\pi \int_0^\infty b db [1 - e^{-\chi_I(s,b)} \cos \chi_R(s,b)], \quad (1)$$

$$\begin{aligned} \sigma_{in}(s) &= \sigma_{tot}(s) - \sigma_{el}(s) = 2\pi \int_0^\infty b db G_{in}(s,b) \\ &= 2\pi \int_0^\infty b db [1 - e^{-2\chi_I(s,b)}], \end{aligned} \quad (2)$$

respectively, where s is the square of the total center-of-mass energy, b is the impact parameter, $G_{in}(s, b)$ is the inelastic overlap function and $\chi(s, b) = \chi_R(s, b) + i\chi_I(s, b)$ is the eikonal function. In this picture the probability that neither hadron is broken up in a collision at impact parameter b is therefore given by $P(s, b) = e^{-2\chi_I(s, b)}$. The eikonal function can be written in terms of even and odd eikonal parts connected by crossing symmetry. Thus, in the case of the proton-proton (pp) and antiproton-proton ($\bar{p}p$) scatterings, this combination reads $\chi_{pp}^{\bar{p}p}(s, b) = \chi^+(s, b) \pm \chi^-(s, b)$.

In the so called Dynamical Gluon Mass model [10, 11] (henceforth referred to as DGM model) the increase of the total cross sections is associated with semihard scatterings of partons in the hadrons, and the high-energy dependence of the cross sections is driven mainly by gluon-gluon scattering processes. In this QCD-inspired model the even eikonal is written as the sum of gluon-gluon, quark-gluon, and quark-quark contributions:

$$\begin{aligned}\chi^+(s, b) &= \chi_{qq}(s, b) + \chi_{qg}(s, b) + \chi_{gg}(s, b) \\ &= i[\sigma_{qq}(s)W(b; \mu_{qq}) + \sigma_{qg}(s)W(b; \mu_{qg}) + \sigma_{gg}(s)W(b; \mu_{gg})],\end{aligned}\quad (3)$$

where $W(b; \mu)$ is the overlap density for the partons at impact parameter space b and $\sigma_{ij}(s)$ are the elementary subprocess cross sections of colliding quarks and gluons ($i, j = q, g$). The overlap density is associated with the Fourier transform of a dipole form factor, $W(b; \mu) = \mu^5 b^3 K_3(\mu b)/96\pi$, where $K_3(x)$ is the modified Bessel function of second kind. The contributions $\chi_{qq}(s, b)$ and $\chi_{qg}(s, b)$ are parametrized with terms dictated by the Regge phenomenology:

$$\chi_{qq}(s, b) = i\Sigma A \frac{m_g}{\sqrt{s}} W(b; \mu_{qq}), \quad (4)$$

$$\chi_{qg}(s, b) = i\Sigma \left[A' + B' \ln \left(\frac{s}{m_g^2} \right) \right] W(b; \mu_{qg}), \quad (5)$$

where μ_{qq} , μ_{qg} , A , A' and B' are fitting parameters. The Σ factor is defined as $\Sigma = 9\pi\bar{\alpha}_s^2(0)/m_g^2$, where $\bar{\alpha}_s$ and m_g are non-perturbative quantities which will be defined in the ensuing text. Since the role of the odd eikonal $\chi^-(s, b)$ is to account for the difference between pp and $\bar{p}p$ channels at low energies, it is simply written as $\chi^-(s, b) = C^- \Sigma \frac{m_g}{\sqrt{s}} e^{i\pi/4} W(b; \mu^-)$, where C^- and μ^- are constants to be fitted. The details concerning the analyticity properties of the model amplitudes are given in Ref. [10].

The last term of the expression (3), the gluon contribution $\chi_{gg}(s, b) = \sigma_{gg}(s)W(b; \mu_{gg})$, deserves a more detailed comment: it gives the main contribution to the asymptotic behavior of hadron-hadron total cross sections; its energy dependence comes from the gluon-gluon cross section

$$\sigma_{gg}(s) = C_{gg} \int_{4m_g^2/s}^1 d\tau F_{gg}(\tau) \hat{\sigma}(\hat{s}), \quad (6)$$

where $\tau = x_1 x_2 = \hat{s}/s$. Here $F_{gg}(\tau) \equiv [g \otimes g](\tau) = \int_{\tau}^1 \frac{dx}{x} g(x) g\left(\frac{\tau}{x}\right)$ is the convoluted structure function for pair gluon-gluon (gg), $\hat{\sigma}(\hat{s})$ is the total cross section for the subprocess $gg \rightarrow gg$, and C_{gg} is a free parameter. Note that since $s \gg m_g$ the dominant contribution to the integration comes from the small- x region. In addition, the dynamical gluon mass scale is a natural regulator for the infrared divergences associated with the gluon-gluon cross section. Since in the model the small- x semihard gluons play a central role, a phenomenological gluon distribution is introduced, namely $g(x) = N_g (1-x)^5/x^J$, where $J = 1 + \epsilon$ and $N_g = \frac{1}{240}(6-\epsilon)(5-\epsilon)\dots(1-\epsilon)$. Note that the gluon distribution reduces to $g(x) = 0$ in the limit $x \rightarrow 1$, as expected by dimensional counting rules. The total cross section $\hat{\sigma}(\hat{s}) = \int_{\hat{t}_{min}}^{\hat{t}_{max}} (d\hat{\sigma}/d\hat{t}) d\hat{t}$ is given by [10, 11]

$$\hat{\sigma}(\hat{s}) = \frac{3\pi\bar{\alpha}_s^2}{\hat{s}} \left[\frac{12\hat{s}^4 - 55M_g^2\hat{s}^3 + 12M_g^4\hat{s}^2 + 66M_g^6\hat{s} - 8M_g^8}{4M_g^2\hat{s}[\hat{s} - M_g^2]^2} - 3 \ln \left(\frac{\hat{s} - 3M_g^2}{M_g^2} \right) \right]; \quad (7)$$

in the above expression $\bar{\alpha}_s$ and M_g are the QCD effective charge and the dynamical gluon mass, respectively, obtained (through the use of the pinch technique) as solutions of the Schwinger-Dyson equations for the gluon propagator and the triple gluon vertex [14]. These non-perturbative effective quantities are given by

$$\bar{\alpha}_s = \bar{\alpha}_s(\hat{s}) = \frac{4\pi}{\beta_0 \ln [(\hat{s}^2 + 4M_g^2(\hat{s}^2))/\Lambda^2]}, \quad (8)$$

$$M_g^2 = M_g^2(\hat{s}) = m_g^2 \left[\frac{\ln \left(\frac{\hat{s}^2 + 4m_g^2}{\Lambda^2} \right)}{\ln \left(\frac{4m_g^2}{\Lambda^2} \right)} \right]^{-12/11}, \quad (9)$$

where $\Lambda (\equiv \Lambda_{QCD})$ is the QCD scale parameter, $\beta_0 = 11 - \frac{2}{3}n_f$ (n_f is the number of flavors), and m_g is an infrared mass scale to be adjusted in order to provide reliable results concerning calculations of strongly interacting processes. As mentioned in the earlier section, the existence of a gluon mass scale is strongly supported by QCD lattice simulations [8], and its

TABLE I. Values of the DGM model parameters from the global fit to the scattering pp and $\bar{p}p$ data.

C_{gg}	$(1.62 \pm 0.37) \times 10^{-3}$
μ_{gg} [GeV]	0.642 ± 0.034
A	9.04 ± 4.94
μ_{qq} [GeV]	1.299 ± 0.797
A'	$(4.68 \pm 1.89) \times 10^{-1}$
B'	$(4.53 \pm 1.94) \times 10^{-2}$
μ_{qg} [GeV]	0.825 ± 0.015
C^-	3.12 ± 0.33
μ^- [GeV]	0.799 ± 0.298
χ^2/DOF	0.98

value is typically found to be of the order $m_g = 500 \pm 200$ MeV [9–11]. It is worth noting that in all these phenomenological studies the mass scale m_g is used as an input parameter. However, it was recently obtained, for the first time, a value for the mass scale m_g from the analysis of the proton structure function $F_2(x, Q^2)$ at small- x [12]. In that work the HERA data on F_2 is interpreted in terms of the generalized double-asymptotic-scaling approximation with a QCD effective charge, and at leading order (LO) the value $m_g = 364 \pm 26$ MeV arises naturally from the analysis. This 90% confidence level uncertainty result, obtained from a global fit to $F_2(x, Q^2)$ data sets through a χ^2 fitting procedure, sets up the stage for making an assessment of the mass scale uncertainty for the hadron-hadron observable to be calculated, as discussed in what follows.

First, in order to determine the DGM model parameters, we set the value of the gluon scale mass to $m_g = 364$ MeV, and fix $n_f = 4$ and $\Lambda = 284$ MeV. These choices are not only consistent to LO procedures, but are also the same ones adopted in Ref. [12]. Then we carry out a global fit to all high-energy forward pp and $\bar{p}p$ scattering data above $\sqrt{s} = 10$ GeV, namely the total cross section $\sigma_{tot}^{pp, \bar{p}p}$, the ratio of the real to imaginary part of the forward scattering amplitude $\rho^{pp, \bar{p}p}$, the elastic differential scattering cross sections $d\sigma^{\bar{p}p}/dt$ at $\sqrt{s} = 546$ GeV and $\sqrt{s} = 1.8$ TeV as well as the recent TOTEM datum on σ_{tot}^{pp} at $\sqrt{s} = 7$ TeV [15]. The values of the fitted parameters are given in Table 1. The χ^2/DOF for the

global fit was 0.98 for 320 degrees of freedom. This result is obtained by fixing the quantity $J = 1 + \epsilon$, which determines the asymptotic behavior of σ_{tot}^{pp} , at $J = 1.21$; it appears to be the optimal value to fit the TOTEM datum on σ_{tot}^{pp} at $\sqrt{s} = 7$ TeV. Interestingly enough, the value $J = 1.21$ is the same value obtained from a recent triple-Regge analysis which explicitly accounts for absorptive corrections [16]. The results of the fits to $\sigma_{tot}^{pp,\bar{p}p}$, $\rho^{pp,\bar{p}p}$ and $d\sigma^{\bar{p}p}/dt$ are displayed in Figs. 1a, 1b and 1c, respectively, together with the experimental data. The hatched areas in Figs. 1a and 1b correspond to the uncertainties in the predictions due to the gluon mass error, namely $\delta m_g = 26$ MeV. In Figure 1d we show the theoretical predictions for the pp differential scattering cross sections at $\sqrt{s} = 7$ and 14 TeV; the comparison of the prediction at $\sqrt{s} = 7$ TeV with the published experimental data [15] shows good agreement.

III. INELASTIC CHANNEL: THE STRING APPROACH

The number n of charged hadrons in the final state of a collision is a basic observable in high-energy processes. Although n is one of the simplest observables in hadron-hadron collisions, being a global measure characterizing final states, it provides important constraints on the mechanism of production of the particles. Accordingly, the charged particle multiplicity distribution P_n , which give us the probability for producing n charged hadrons in a given event, is the most general characteristic of multi-particle production processes. The multiplicity distribution P_n follows a Poisson distribution in the case of independent production of the final-state particles, but deviations from the Poisson shape contains information about multi-particle correlations [1, 5]. Higher-order moments of P_n , which measure the event-to-event multiplicity fluctuations, constitute a powerful tool for studying these correlations. Measurements of the s dependence of P_n and its moments has been used to improve or reject models of particle production.

The multiplicity distributions are usually represented in terms of the Koba-Nielsen-Olesen (KNO) function $\Phi(z) \equiv \langle n \rangle P_n$, where $\langle n \rangle$ is the mean of the multiplicity distribution and $z = n/\langle n \rangle$. It is experimentally observed that for hadron-hadron collisions the KNO function $\Phi(z)$ is approximately independent of s (KNO scaling) over the ISR energy range and shows dramatic scaling violation from ISR to FNAL and LHC energies. In these collisions the production of minijets from semihard partonic processes becomes increasingly important at high energies, and in many theoretical approaches the minijets are the responsible not

only for the rapid growth of hadron-hadron cross sections but also for the violation of the KNO scaling. This renders the DGM model particularly adept at calculating P_n and its moments, since in the model the increase of the pp and $\bar{p}p$ total cross sections as well as the violation of KNO scaling is driven especially by the semihard component of the eikonal model [10, 11, 17, 18].

A reliable approach for the calculation of the multiplicity distribution, using the DGM model, can be established by exploring the unitarity condition of the S -matrix in the following way: the elastic scattering amplitude, in the impact parameter b space, may be written

$$2\text{Re}\Gamma(s, b) = |\Gamma(s, b)|^2 + G_{in}(s, b), \quad (10)$$

where $\Gamma(s, b)$ is the profile function and $G_{in}(s, b)$ the inelastic overlap function. From the optical theorem we obtain $\sigma_{tot}(s) = 2 \int d^2b \text{Re}\Gamma(s, b)$, and since the function $G_{in}(s, b)$ represents the probability of absorption associated to each b value, we get the total inelastic cross section $\sigma_{in}(s) = \int d^2b G_{in}(s, b)$. Thus the unitarity condition (10) is equivalent to $\sigma_{tot}(s) = \sigma_{el}(s) + \sigma_{in}(s)$, where $\sigma_{el}(s) = \int d^2b |\Gamma(s, b)|^2$. The multiplicity distribution $P_n(s)$, the probability of producing n charged particles in an inelastic collision at the energy s , is given by

$$P_n(s) = \frac{\sigma_n(s)}{\sigma_{in}(s)}, \quad (11)$$

where $\sigma_n(s)$ is the n -particle topological cross section, with $\sum_n \sigma_n(s) = \sigma_{in}(s)$. The connection between the multiplicity distribution and the DGM eikonal becomes complete using a phenomenological procedure referred to as *geometrical* or *string approach* [17–21], where the hadronic multiplicity $P_n(s)$ can be constructed in terms of elementary quantities related to microscopic processes. More specifically, the topological cross section is written as

$$\sigma_n(s) \equiv \int d^2b \sigma_n(s, b) = \int d^2b G_{in}(s, b) \left[\frac{\sigma_n(s, b)}{\sigma_{in}(s, b)} \right], \quad (12)$$

since $\sigma_{in}(s) \equiv \int d^2b \sigma_{in}(s, b) = \int d^2b G_{in}(s, b)$. In this way the multiplicity distribution $P_n(s)$ is given by

$$P_n(s) = \frac{1}{\sigma_{in}(s)} \int d^2b \frac{G_{in}(s, b)}{\langle n(s, b) \rangle} [\langle n(s, b) \rangle p_n(s, b)], \quad (13)$$

where $\langle n(s, b) \rangle$ is the average number of particles produced at b and s , and $p_n(s, b) \equiv \sigma_n(s, b)/\sigma_{in}(s, b)$. Let $\Phi(s, z) = \langle n(s) \rangle P_n(s)$ be the overall multiplicity distribution, where

$z = n(s)/\langle n(s) \rangle$ is the corresponding KNO variable. A multiplicity distribution $\phi(s, \underline{z})$, associated with elementary processes occurring at b and s , can be written in the form $\phi(s, \underline{z}) = \langle n(s, b) \rangle p_n(s, b)$, where $\underline{z} = n(s)/\langle n(s, b) \rangle$. Note that both distributions obey the usual normalizations [22, 23]

$$\int_0^\infty dz \Phi(z) = \int_0^\infty d\underline{z} \phi(\underline{z}) = 2 \quad (14)$$

and

$$\int_0^\infty dz z \Phi(z) = \int_0^\infty d\underline{z} \underline{z} \phi(\underline{z}) = 2. \quad (15)$$

In this approach the average number of particles $\langle n(s, b) \rangle$ factorizes as $\langle n(s, b) \rangle = \langle n(s) \rangle f(s, b)$, and therefore the expression (13) can be rewritten in the KNO form

$$\Phi(s, z) = \langle n(s) \rangle P_n(s) = \frac{1}{\int d^2b G_{in}(s, b)} \int d^2b \frac{G_{in}(s, b)}{f(s, b)} \phi\left(\frac{z}{f(s, b)}\right), \quad (16)$$

where $f(s, b)$ is a *multiplicity function* to be defined. Thus the connection between $\Phi(s, z)$ and the DGM eikonal can finally be established since, as shown in the expression (2), the inelastic overlap function is simply $G_{in}(s, b) = 1 - e^{-2\chi_I(s, b)}$. Therefore

$$P_n(s) = \frac{1}{\langle n(s) \rangle \int d^2b [1 - e^{-2\chi_I(s, b)}]} \int d^2b \frac{[1 - e^{-2\chi_I(s, b)}]}{f(s, b)} \phi^{(1)}\left(\frac{z}{f(s, b)}\right), \quad (17)$$

where we have introduced an index labeling the function ϕ in order to stress the underlying assumption of the string approach: the hadronic multiplicity $P_n(s)$ is obtained by summing contributions from parton-parton interactions occurring at fixed b and s , with the subsequent creation, per collision, of an object like a string. These strings give rise to parton cascades followed by the non-perturbative hadronization phase transition, where the partons become the hadrons which are experimentally observed. In our case each string has equal probability of turning into a pair of charged hadrons.

It is well known that over a large range of energies the experimental data on multiplicity distributions are well fitted by the Negative Binomial Distribution (NBD). Hence, in this work we take the KNO form of the NBD, or Gamma distribution,

$$\phi^{(1)}(z) = 2 \frac{K^K}{\Gamma(K)} z^{K-1} e^{-Kz}, \quad (18)$$

as the parametrization of the elementary multiplicity distribution $\phi^{(1)}$. This choice allows for a natural interpretation of the parameter K as a dimensionless minimum length for a

multitude of string-like objects, as discussed by Barshay many years ago [24]. Moreover, the Gamma distribution arises as the dominant part of the solution of the equation for three-gluon branching in the very-large- n limit [25]; this branching equation, which takes into account only gluon bremsstrahlung process, gives the main contribution at high energies since semihard gluons dominate the parton-parton cross sections. Curiously enough, from the color glass condensate approach the NBD appears to be the underlying distribution of gluon multiplicities arising from electric and magnetic flux tubes in the Glasma [26].

In addition, it has been assumed that the energy effectively employed for the production of particles in a given interaction is proportional to the eikonal [17–22, 24]. It means that the eikonal may be interpreted as a measure of the effective overlap of two colliding matter distributions on the impact parameter plane. As a result, since the high-energy eikonal is largely imaginary, we adopt the following form for the multiplicity function $f(s, b)$:

$$f(s, b) = \xi(s) [\chi_I(s, b)]^{2\zeta}, \quad (19)$$

where the relation

$$\xi(s) = \frac{\int d^2b [1 - e^{-2\chi_I(s, b)}]}{\int d^2b [1 - e^{-2\chi_I(s, b)}] [\chi_I(s, b)]^{2\zeta}} \quad (20)$$

is determined by the normalization condition (15). Since the eikonal $\chi_I(s, b)$ is completely determined from the elastic fit, we see from Eqs. (18) and (19) that the only free parameters in Eq. (17) are K and ζ . Further, for our purposes it is sufficient to fix the value of K and assume ζ as the single fitting parameter; in Refs. [18] and [19] it is shown that the choice $K = 10.775$ gives good descriptions of the charged multiplicity distributions for e^+e^- annihilation data in a large interval of $\sqrt{s_{e^+e^-}}$. Moreover, our assumption that each string has equal probability of turning into hadrons suggests a common minimum length K for different pp and $\bar{p}p$ centre-of-mass energies. More important, this procedure in fact does provide an excellent description of P_n data at high multiplicities, avoiding the introduction of more free parameters, as it is shown in the sequence.

In order to determine the parameter ζ , we set the value of the dimensionless length to $K = 10.775$, and carry out fits to full phase space P_n data over a large range of energies, namely at $\sqrt{s} = 30.4, 44.5, 52.6, 62.2, 300, 546, 1000$ and 1800 GeV [27, 28]. For energies $\sqrt{s} \geq 300$ GeV we have used data from the E735 Collaboration since it is statistically more reliable in the high multiplicity region [28]. It is worth mentioning that it is the region clearly sensitive to the gluon distribution at small- x , and therefore to the underlying mechanisms

TABLE II. Values of the ζ parameter resulting from fits to the P_n data. The values of $\xi(s)$ were obtained from Eq. (20). At ISR energies the values of $\langle n(s) \rangle$ were inputed from Ref. [27], while in the other energies have been obtained from empirical P_n data by using $\langle n \rangle = \sum n P_n$. At LHC energies the values were estimated from Eq. (22).

\sqrt{s} [GeV]	ζ	$\xi(s)$	$\langle n(s) \rangle$	χ^2/DOF
30.4	0.239 ± 0.011	1.642	9.43	0.588
44.5	0.240 ± 0.011	1.643	10.86	0.306
52.6	0.239 ± 0.009	1.639	11.55	0.765
62.2	0.231 ± 0.008	1.613	12.25	1.717
300	0.263 ± 0.003	1.589	24.47	0.608
546	0.305 ± 0.004	1.599	29.53	0.300
1000	0.288 ± 0.005	1.508	38.46	1.469
1800	0.315 ± 0.002	1.468	44.82	0.782
7000	0.352	1.308	81.79	—
14000	0.372	1.209	108	—

of the DGM model. In all these fits we use a χ^2 fitting procedure with an interval $\chi^2 - \chi_{min}^2$ corresponding to the projection of the χ^2 hypersurface containing 90% of probability. The parameter values obtained in each fit, as well as the associated $\xi(s)$ and $\langle n(s) \rangle$ values, are given in Table II.

The theoretical prediction to P_n at LHC energies can be computed by fitting the energy behavior of ζ through an appropriate function $\zeta(s)$. As can be seen from the Figure 2, the parameter increases rapidly with s , being its energy dependence described in a consistent way through the use of the function

$$\zeta(s) = a + b \ln^c(s), \quad (21)$$

where $a=0.189$, $b=0.00197$ and $c=1.536$; these values were obtained by a χ^2 analysis. From the curve depicted in Fig. 2 it is possible to extract the values of ζ at 7 and 14 TeV shown in the Table II. In the same way, the values of the hadronic average multiplicity at LHC energies can be estimated using the equation introduced by Troshin and Tyurin [29]

$$\langle n(s) \rangle = 2.328 s^{0.201}, \quad (22)$$

which is in very good agreement with experimental data.

The results of the fits to P_n data are displayed in Figs. 3 and 4, together with the experimental data. In Figure 4 the hatched areas correspond to the uncertainties in the predictions due to the gluon mass error. Notice that, since at ISR energies gluon-gluon processes are not dominant, the widths of uncertainties bands in Figure 3 are very narrow. In Figure 5 we show the theoretical predictions for the full-phase-space multiplicity distribution at $\sqrt{s} = 7$ and 14 TeV, together with data, from CMS, on fully corrected charged hadron multiplicity spectrum for $|\eta| < 0.5, 1.0, 1.5, 2.0$ and 2.4 at $\sqrt{s} = 7$ TeV [30].

Information about multi-particle correlations can be extracted directly from the shape of the multiplicity distribution P_n . As first indicated in the Section III, independent production of the particles in the final state leads to a Poissonian multiplicity distribution. However, deviations from this Poisson shape reveal correlations among the produced particles and unveil many details about the underlying dynamics.

The shape of a distribution can be analyzed by studying its moments. In the case of the multiplicity distribution P_n , its factorial moments F_q as well as its cumulant factorial moments K_q are powerful tools to investigate multiplicity fluctuations [1, 31–34]. The normalized factorial moment of rank q is defined by

$$F_q = \frac{1}{\langle n \rangle^q} \sum_{n=q}^{\infty} n(n-1)\dots(n-q+1) P_n, \quad (23)$$

where $\langle n \rangle = \sum_n n P_n$ is the average multiplicity and q is the rank of the moment. Thus F_q , that reflects correlations among up to q produced particles, is sensitive to the tail of the distribution, i.e. to large n values. For independent production of particles the moment F_q is equal to unity for all rank q . On the other hand, if the produced particles are correlated (anti-correlated), the distribution is broader (narrower) than the Poisson one, and, as a consequence, F_q is greater (less) than unity. The normalized factorial cumulants K_q , obtained from the recursive relation

$$K_q = F_q - \sum_{m=1}^{q-1} \frac{(q-1)!}{m!(q-m-1)!} K_{q-m} F_m \quad (24)$$

with $F_0 = F_1 = K_1 = 1$, measure genuine q -particle correlations, more specifically correlations of rank q which are not a consequence of lower-order correlation functions. It is observed that the factorial and cumulant moments increase rapidly with q and, therefore,

the ratio [35, 36]

$$H_q = \frac{K_q}{F_q} \quad (25)$$

turns out to be a convenient quantity to work with since it have a flatter behavior with q over a large range. Moreover, higher-order QCD calculations predict that the cumulant and H_q moments oscillate as a function of q [35–37]. These predictions have been fully confirmed by high-energy scattering experiments in e^+e^- , pp , $\bar{p}p$, hadron-nucleus and nucleus-nucleus collisions [38]. Namely, QCD results are concerned with partons, not with hadrons. In fact, the H_q moments of *parton* multiplicity distributions are predicted to oscillate. However, H_q moments of experimental data on *hadron* multiplicity distributions exhibit the same oscillatory behavior. This experimental observation strongly suggests the validity of the Local Parton Hadron Duality (LPHD) hypothesis [39, 40], which asserts that parton multiplicity distributions, calculated using perturbative QCD, must be related to the hadronic distributions, implying that the hadronization phase transition does not affect in an essential way the observed final-state hadron distributions.

We have analyzed the H_q moments over a large range of the rank q . First, the theoretical values of P_n are obtained from the Eqs. (17)-(20). Then the F_q , K_q and H_q moments are determined from both the theoretical and the experimental values of P_n according to Eqs. (23)-(25). The results are displayed in Figs. 6 and 7. Our prediction for the H_q moment at the LHC energy $\sqrt{s} = 14$ TeV is presented in Fig. 8. All these results are in good agreement with the experimental points up to $q=16$, i.e., are reliable even on the tail of the distribution.

IV. CONCLUDING REMARKS

In this paper we have explored the unitarity condition of the S -matrix in impact parameter space to describe, in a connected way, hadron-hadron observables in both elastic and inelastic channels. In the elastic channel we have performed a global fit to the pp and $\bar{p}p$ forward quantities σ_{tot} and ρ , including in the dataset the $\bar{p}p$ differential cross section at $\sqrt{s} = 546$ GeV and $\sqrt{s} = 1.8$ TeV as well as the new TOTEM datum on σ_{tot}^{pp} at $\sqrt{s} = 7$ TeV. The analysis was carried out using the DGM eikonal model, where non-perturbative effects are naturally included via a QCD effective charge dependent on the dynamical gluon mass. With the dynamical gluon mass set at $m_g = 364$ MeV, the DGM model allows us to describe successfully all experimental data. Namely, the χ^2/DOF for the global fit was 0.98

for 320 degrees of freedom. This good statistical result shows that the DGM model is well suited for detailed predictions of the forward quantities to be measured at higher energies. In particular, for the total cross sections to be measured at CERN-LHC energies, the model predicts the values $\sigma_{tot}^{pp} = 98.6_{-5.2}^{+6.8}$ mb, $101.1_{-5.4}^{+7.0}$ mb and $112.4_{-6.4}^{+8.1}$ mb, at $\sqrt{s} = 7, 8$ and 14 TeV, respectively. The uncertainty in these total cross sections have been estimated by varying the gluon mass scale within error while keeping all other model parameters constant. Note that this procedure does not determines the *formal* uncertainty in the σ_{tot} prediction, since the variance-covariance matrix method, necessary for proving this quantity, was not employed. However, at high energies the total cross sections are dominated by gluon-gluon interactions represented by the eikonal term $\chi_{gg}(s, b)$, containing only 2 free parameters (C_{gg} and μ_{gg}). It is seen from our χ^2 analysis that the correlation coefficients of these parameters are small. Moreover, the values of the total cross sections are actually more sensitive to the gluon mass scale than to variations of others parameters of the model. Hence, despite the simplicity of the procedure, it clearly provides a good estimate of the full systematic uncertainty in σ_{tot} .

In order to compute multiplicity distributions in pp and $\bar{p}p$ collisions we have adopted the string approach, which enables linkage between the elastic and inelastic channels. This phenomenological approach asserts that P_n in full phase space can be constructed by summing contributions from parton-parton collisions, occurring at b and s . These collisions give rise to the formation of strings and its subsequent fragmentation into hadrons. More specifically, the semihard partons produced at the interaction point fly away from each other yielding a color string which breaks up producing the observed hadrons, a process well described by the conventional Lund model [41]. Thus in this picture the multiplicity distribution P_n can be constructed in terms of the eikonal $\chi_I(s, b)$, which contains the gluon semihard contribution $\chi_{gg}(s, b)$, and of the parameters K and ζ , characterizing the dimensionless length of string-like objects and the *strength* of the KNO scaling violation, respectively. In fact, the parameter ζ is approximately constant at ISR energies, increasing rapidly with s from ISR to LHC energies: this behavior is consistent with KNO scaling hypothesis at $\sqrt{s} \lesssim 100$ GeV and it's violation at higher energies. We call attention in particular to the fact that the multiplicity distribution data are fitted adequately using only one free parameter, since the K as well as the elastic parameters are all fixed.

We point out that the bumpy structure in $P_n(s)$ data at higher energies, which appears in

the region of low multiplicities, can be described by our model by means of a moment analysis which separates the semihard and soft components of the multiplicity distributions. In this analysis the bumpy structure is reproduced after an appropriate convolution of the soft and the semihard components of the eikonal. However, at least one more free parameter is needed. Since our approach aims to achieve a description of the data relying on the smallest number of parameters possible, the description of the bumpy structure is out of the scope of this work.

Concerning the moments and cumulants, we see that our approach describes very well the energy dependence of the F -moments, and reproduce the H_q versus q oscillations observed in the experimental data. More importantly, we observe that the semihard portion of the eikonal is in fact the responsible for the H_q oscillations since it gives the main contribution to high multiplicities, as qualitatively predicted by QCD.

It is worth noting that the unitarity condition of the S -matrix can be also associated with low- x saturation effects of $xG(x, Q^2, |\vec{b}|)$, the b -dependent integrated gluon distribution [42]. These saturation effects appears in a functional integral approach to high-energy scattering in the eikonal representation, and the S -matrix unitarity is preserved as the result of a matrix cumulant expansion and the Gaussian approximation of the functional integrals. In this non-perturbative approach an *effective* gluon mass is introduced, indicating that the underlying physics is similar to that of the DGM model. It corroborates the idea that the non-perturbative dynamics of QCD generate an effective gluon mass at very low Q^2 region.

ACKNOWLEDGMENTS

We thank V.A. Khoze, M.J. Menon, A.A. Natale, F.S. Navarra and E.K.G. Sarkisyan for helpful discussions. This research was partially supported by the Fundação de Amparo à Pesquisa do Estado do Rio Grande do Sul (FAPERGS) and by Coordenação de Aperfeiçoamento de Pessoal de Nível Superior (CAPES).

-
- [1] I.M. Dremin and J.W. Gary, Phys. Rep. **349**, 301 (2001).
 - [2] Yu.L. Dokshitzer, V.A. Khoze, A.H. Mueller, and S.I. Troyan, *Basics of Perturbative QCD* (Editions Frontieres, Gif-sur-Yvette, 1991).

- [3] Yu.L. Dokshitzer, V.A. Khoze, S.I. Troian and A.H. Mueller, *Rev. Mod. Phys.* **60**, 373 (1988).
- [4] S.L.C. Barroso, *et al.*, *Nucl. Phys. B (Proc. Suppl.)* **75**, 150 (1999).
- [5] Jan Fiete Grosse-Oetringhaus and Klaus Reygers, *J. Phys. G* **37**, 083001 (2010).
- [6] W. Kittel and E.A. De Wolf, *Soft Multihadron Dynamics* (World Scientific, 2005)
- [7] L.V. Gribov, E.M. Levin, and M.G. Ryskin, *Phys. Rep.* **100**, 1 (1983); E.M. Levin and M.G. Ryskin, *Phys. Rep.* **189**, 267 (1990).
- [8] F.D.R. Bonnet, P.O. Bowman, D.B. Leinweber, A.G. Williams, and J.M. Zanotti, *Phys. Rev. D* **64**, 034501 (2001); A. Cucchieri, T. Mendes, and A. Taurines, *Phys. Rev. D* **67**, 091502(R) (2003); P.O. Bowman, U.M. Heller, D.B. Leinweber, M.B. Parappilly, and A.G. Williams, *Phys. Rev. D* **70**, 034509 (2004); A. Sternbeck, E.-M. Ilgenfritz, and M. Muller-Preussker, *Phys. Rev. D* **73**, 014502 (2006); Ph. Boucaud, *et al.*, *J. High Energy Phys.* 0606 (2006) 001; P.O. Bowman, *et al.*, *hep-lat/0703022*; I.L. Bogolubsky, E.M. Ilgenfritz, M. Muller-Preussker, and A. Sternbeck, *Phys. Lett B* **676**, 69 (2009); O. Oliveira, P. J. Silva, *arXiv:0911.1643* [hep-lat]; A. Cucchieri, T. Mendes, and E.M.S. Santos, *Phys. Rev. Lett.* **103**, 141602 (2009); A. Cucchieri and T. Mendes, *Phys. Rev. D* **81**, 016005 (2010); D. Dudal, O. Oliveira, and N. Vandersickel, *Phys. Rev. D* **81**, 074505 (2010); A. Cucchieri, D. Dudal, T. Mendes, and N. Vandersickel, *arXiv:1202.0639* [hep-lat].
- [9] F. Halzen, G. Krein, A.A. Natale, *Phys. Rev. D* **47**, 295 (1993); M.B. Gay Ducati, F. Halzen, A.A. Natale, *Phys. Rev. D* **48**, 2324 (1993); A.C. Aguilar, A. Mihara, A.A. Natale, *Phys. Rev. D* **65**, 054011 (2002); E.G.S. Luna, A.A. Natale, C.M. Zanetti, *Int. J. Mod. Phys. A* **23**, 151 (2008); A.A. Natale and C.M. Zanetti, *Int. J. Mod. Phys. A* **24**, 4133 (2009).
- [10] E.G.S. Luna, A.F. Martini, M.J. Menon, A. Mihara, A.A. Natale, *Phys. Rev. D* **72**, 034019 (2005).
- [11] E.G.S. Luna, *Phys. Lett. B* **641**, 171 (2006); E.G.S. Luna, A.A. Natale, *Phys. Rev. D* **73**, 074019 (2006); E.G.S. Luna, *Braz. J. Phys.* **37**, 84 (2007); D.A. Fagundes, E.G.S. Luna, M.J. Menon, and A.A. Natale, *Nucl. Phys. A* **886**, 48 (2012).
- [12] E.G.S. Luna, A.L. dos Santos, and A.A. Natale, *Phys. Lett. B* **698**, 52 (2011).
- [13] A. Corsetti, A. Grau, G. Pancheri, and Y.N. Srivastava, *Phys. Lett. B* **382**, 282 (1996); A. Grau, G. Pancheri, and Y.N. Srivastava, *Phys. Rev. D* **60**, 114020 (1999); R.M. Godbole, A. Grau, G. Pancheri, and Y.N. Srivastava, *Phys. Rev. D* **72**, 076001 (2005); A. Achilli *et al.*, *Phys. Lett. B* **659**, 137(2008); A. Grau, R.M. Godbole, G. Pancheri, and Y.N. Srivastava,

- Phys. Lett. B **682**, 55 (2009); G. Pancheri, D.A. Fagundes, A. Grau, S. Pacetti, and Y.N. Srivastava, arXiv:1301.2925 [hep-ph].
- [14] J.M. Cornwall, Phys. Rev. D **26**, 1453 (1982); J.M. Cornwall and J. Papavassiliou, Phys. Rev. D **40**, 3474 (1989); J. Papavassiliou and J.M. Cornwall, Phys. Rev. D **44**, 1285 (1991).
 - [15] G. Antchev, *et al.*, Europhys. Lett. **101**, 21002 (2013).
 - [16] E.G.S. Luna, V.A. Khoze, A.D. Martin, and M.G. Ryskin, Eur. Phys. J. C **59**, 1 (2009); **69**, 95 (2010).
 - [17] P.C. Beggio, Nucl. Phys. A **913**, 264 (2013).
 - [18] P.C. Beggio, Nucl. Phys. A **864**, 140 (2011).
 - [19] P.C. Beggio, M.J. Menon, and P. Valin, Phys. Rev. D **61**, 034015 (2000).
 - [20] P.C. Beggio and Y. Hama, Braz. J. Phys. **37**, 1164 (2007).
 - [21] P.C. Beggio, Braz. J. Phys. **38**, 598 (2008).
 - [22] S. Barshay, Phys. Lett. B **116**, 193 (1982); Phys. Rev. Lett. **49**, 1609 (1982).
 - [23] C.S. Lam and P.S. Yeung, Phys. Lett. B **119**, 445 (1982).
 - [24] S. Barshay, Mod. Phys. Lett. A **2**, 693 (1987).
 - [25] B. Durand and I. Sarcevic, Phys. Lett. B **172**, 104 (1986); Phys. Rev. D **36**, 2693 (1987).
 - [26] F. Gelis, T. Lappi, and L. McLerran, Nucl. Phys. A **828** (2009) 149.
 - [27] A. Breakstone *et al.*, Phys. Rev. D **30**, 528 (1984).
 - [28] T. Alexopoulos *et al.*, Phys. Lett. B **435**, 453 (1998).
 - [29] S.M. Troshin and N.E. Tyurin, Int. J. Mod. Phys. A **26**, 4703 (2011).
 - [30] V. Khachatryan *et al.*, J. High Energy Phys. **01**, 079 (2011).
 - [31] W. Kittel, S.V. Chekanov, D.J. Mangeol, and W.J. Metzger, Nucl. Phys. B (Proc. Suppl.) **71**, 90 (1999).
 - [32] A. Giovannini and R. Ugoccioni, Nucl. Phys. B (Proc. Suppl.) **64**, 68 (1998).
 - [33] P. Achard, *et al.*, Phys. Lett. B **577**, 109 (2003).
 - [34] E.K.G. Sarkisyan, Phys. Lett. B **477**, 1 (2000).
 - [35] I.M. Dremin and V.A. Nechitailo, JETP Lett. **58**, 881 (1993).
 - [36] I.M. Dremin and R.C. Hwa, Phys. Rev. D **49**, 5805 (1994).
 - [37] I.M. Dremin, Phys. Lett. B **313**, 209 (1993).
 - [38] J. Dias de Deus, C. Pajares, and C.A. Salgado, Phys. Lett. B **407**, 335 (1997).
 - [39] Ya.I. Azimov, Yu.L. Dokshitzer, V.A. Khoze, and S.I. Troyan, Z. Phys. C **27**, 65 (1985); **31**,

- 213 (1986).
- [40] V.A. Khoze and W. Ochs, Int. J. Mod. Phys. A **12**, 2949 (1997).
- [41] B. Andersson, G. Gustafson, G. Ingelman, and T. Sjostrand, Phys. Rept. **97**,31 (1983); B. Andersson, G. Gustafson, and B. Soderberg, Z. Phys. C **20**, 317 (1983).
- [42] A.I. Shoshi, F.D. Steffen, and H.J. Pirner, arXiv:0205343 [hep-ph]; A.I. Shoshi and F.D. Steffen, arXiv:0212070 [hep-ph]; A.I. Shoshi, F.D. Steffen, and H.J. Pirner, Nucl. Phys. A **709**, 131 (2002).

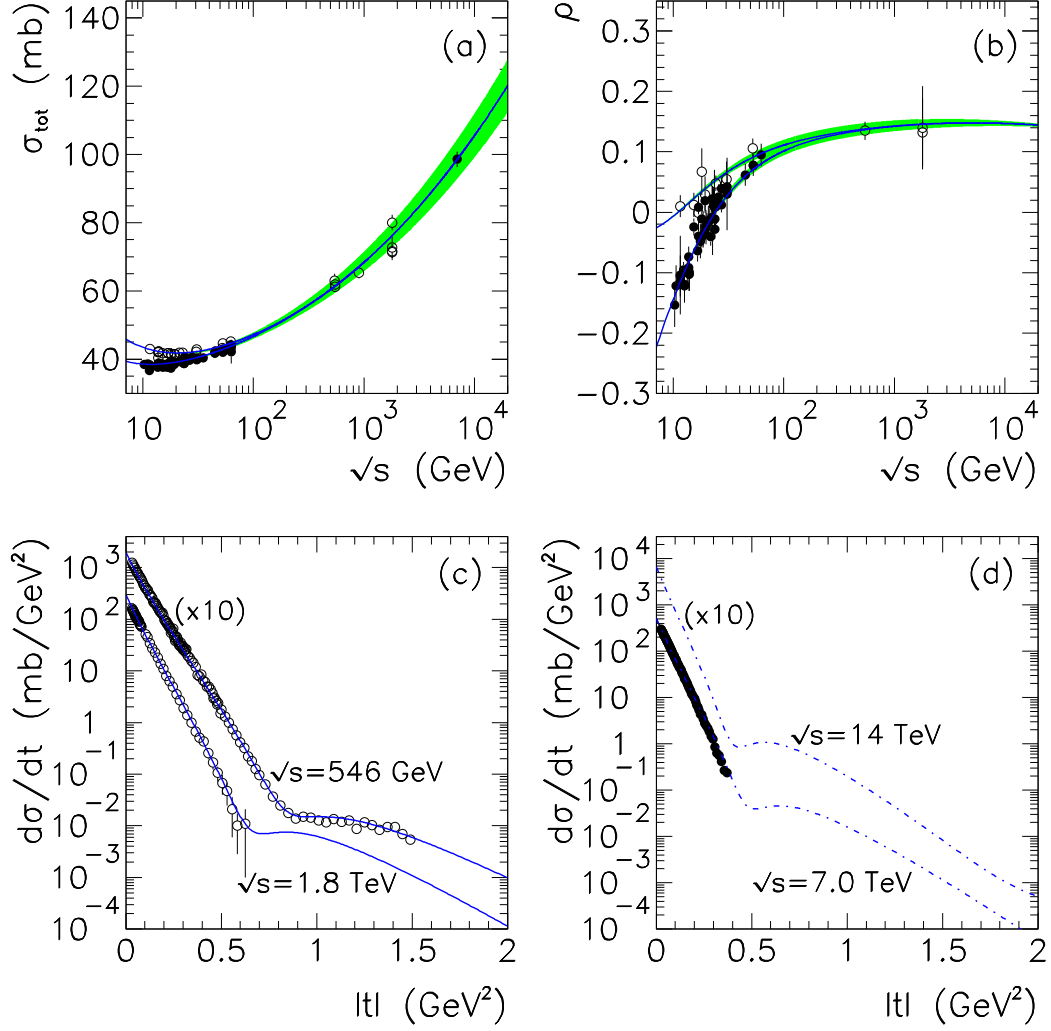


FIG. 1. (a) Total cross section, (b) ratio of the real to imaginary part of the forward scattering amplitude, and (c) elastic differential scattering cross sections for pp (\bullet) and $\bar{p}p$ (\circ). In (d) we show the theoretical predictions for $d\sigma^{pp}/dt$ at $\sqrt{s} = 7$ and 14 TeV. The hatched areas in (a) and (b) correspond to the uncertainties in the predictions due to the gluon mass error.

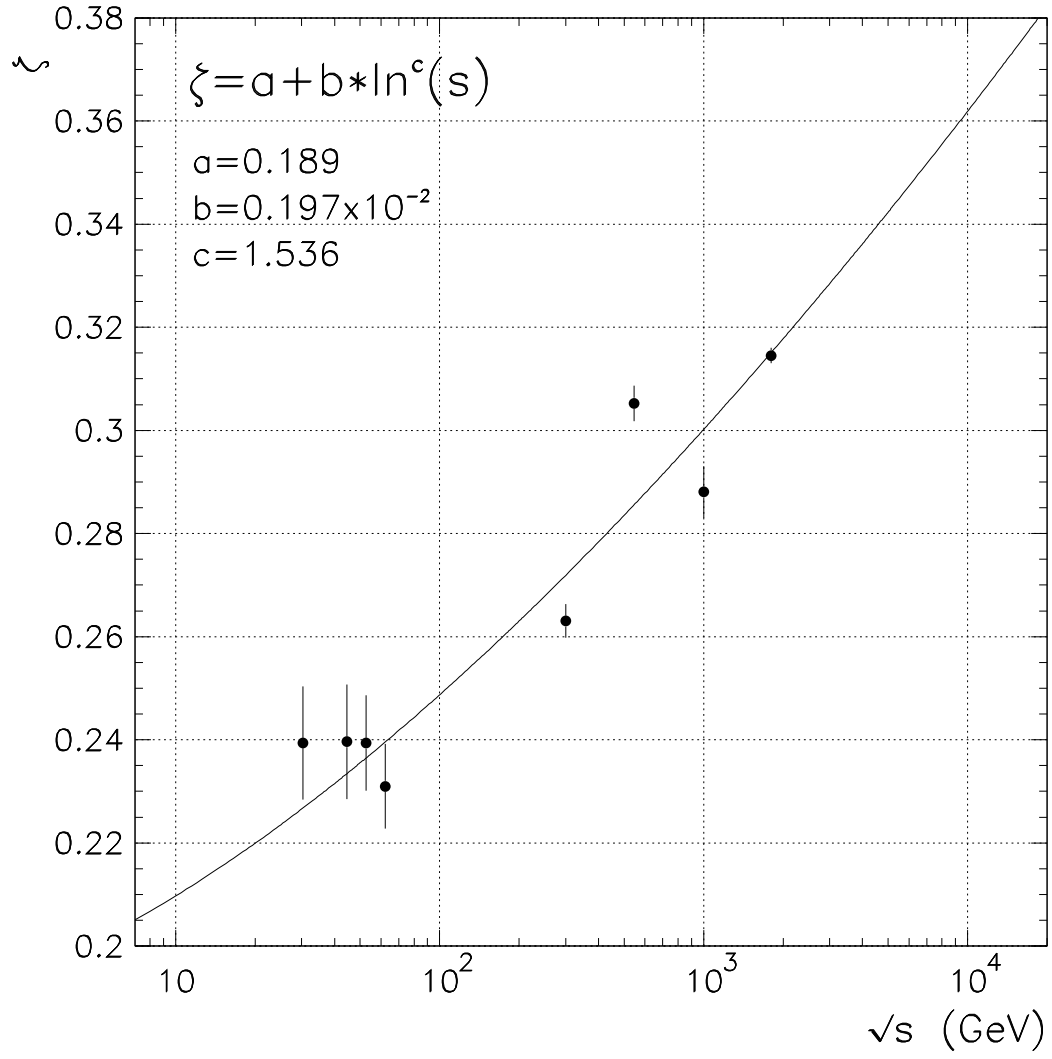


FIG. 2. The energy dependence of the parameter ζ .

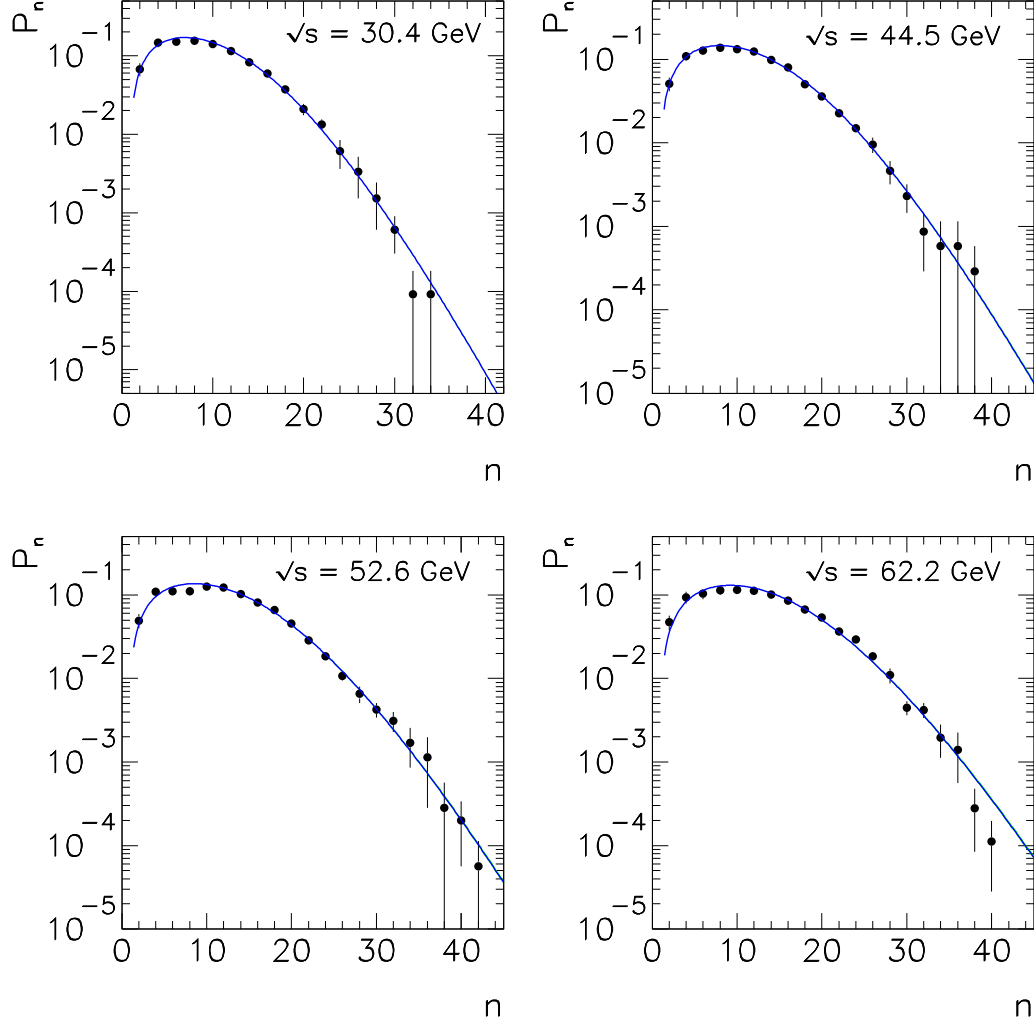


FIG. 3. Multiplicity distributions for inelastic pp data at $\sqrt{s} = 30.4, 44.5, 52.6$ and 62.2 GeV compared with theoretical expectations.

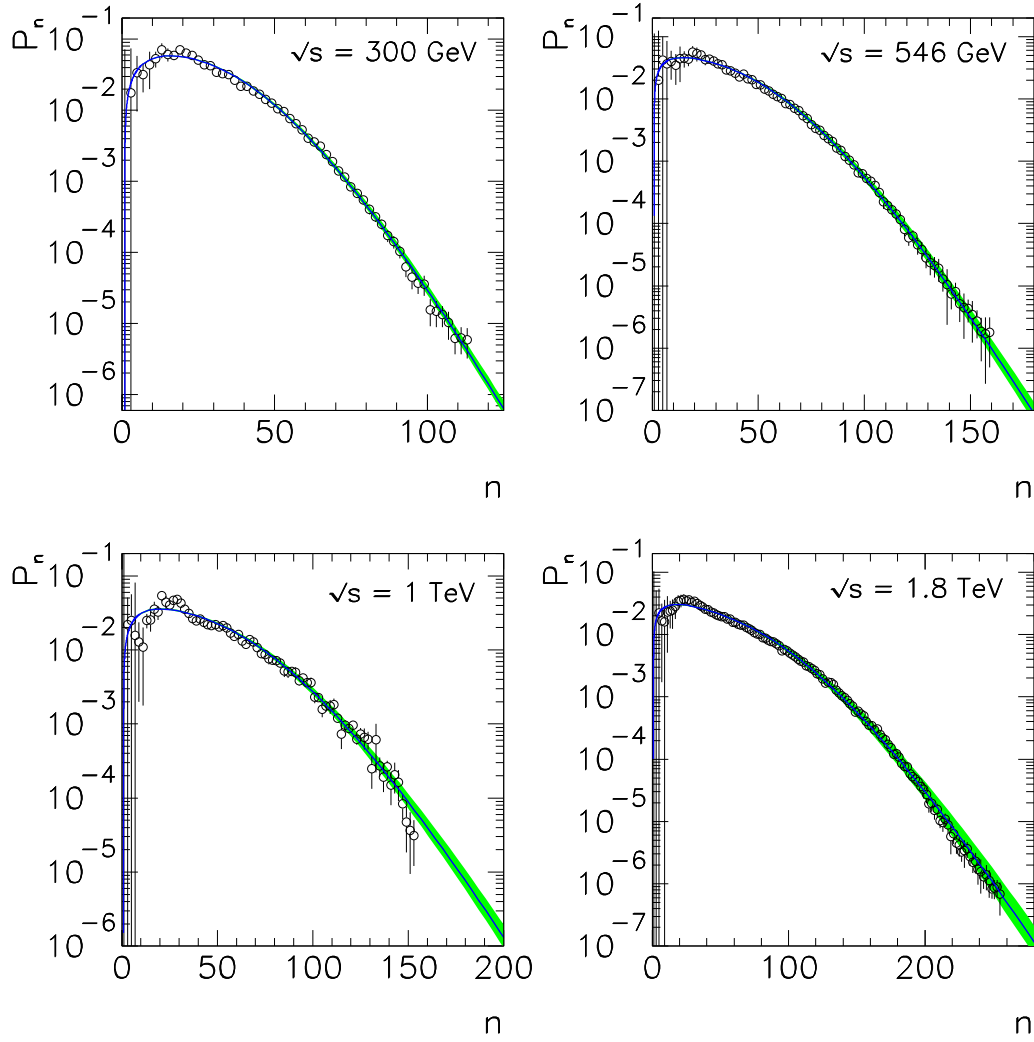


FIG. 4. Multiplicity distributions for inelastic $\bar{p}p$ data at $\sqrt{s} = 300, 546, 1000$ and 1800 GeV compared with theoretical expectations. The hatched areas correspond to the uncertainties in the predictions due to the gluon mass error.

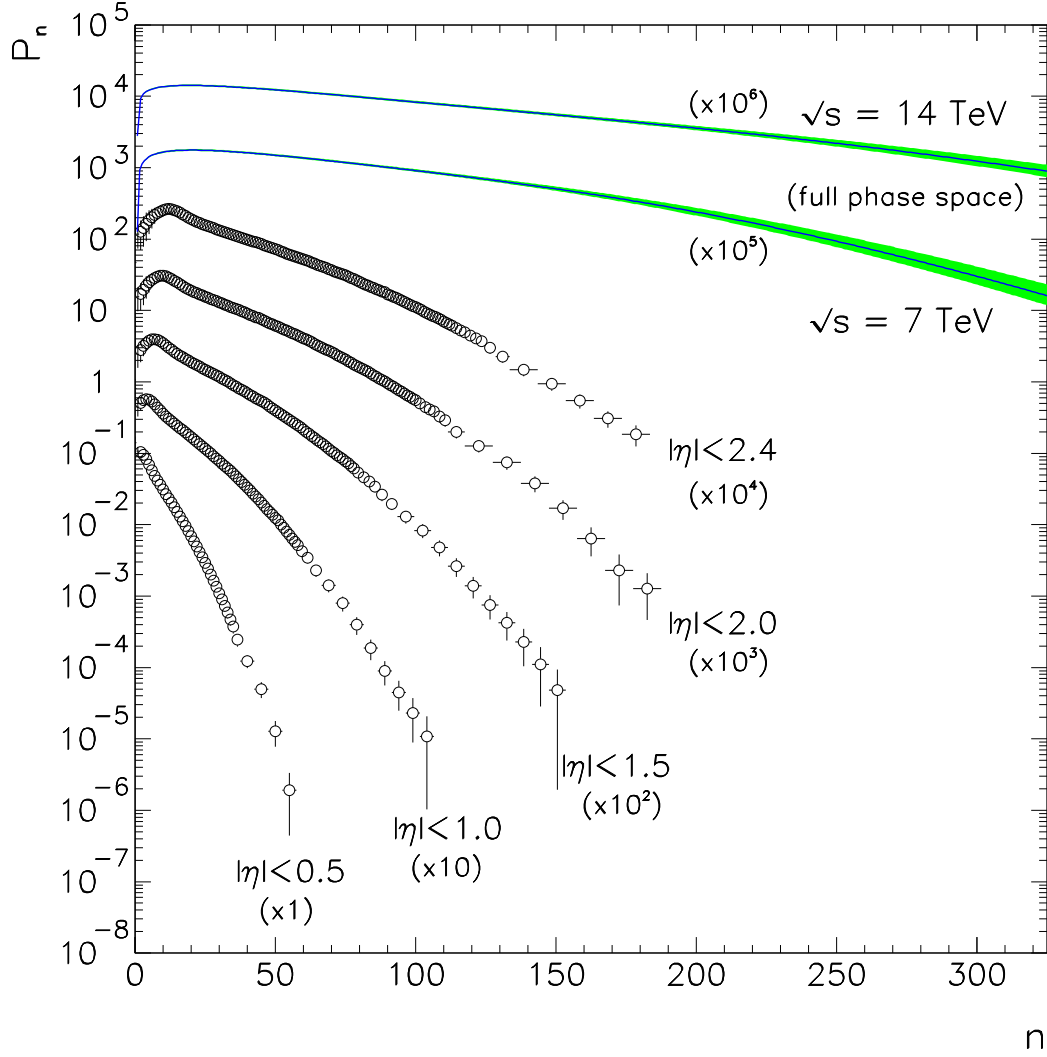


FIG. 5. Theoretical predictions for the full-phase-space multiplicity distribution at $\sqrt{s} = 7$ and 14 TeV, together with data on charged hadron multiplicity spectrum for $|\eta| < 0.5, 1.0, 1.5, 2.0$ and 2.4 at $\sqrt{s} = 7$ TeV [30].

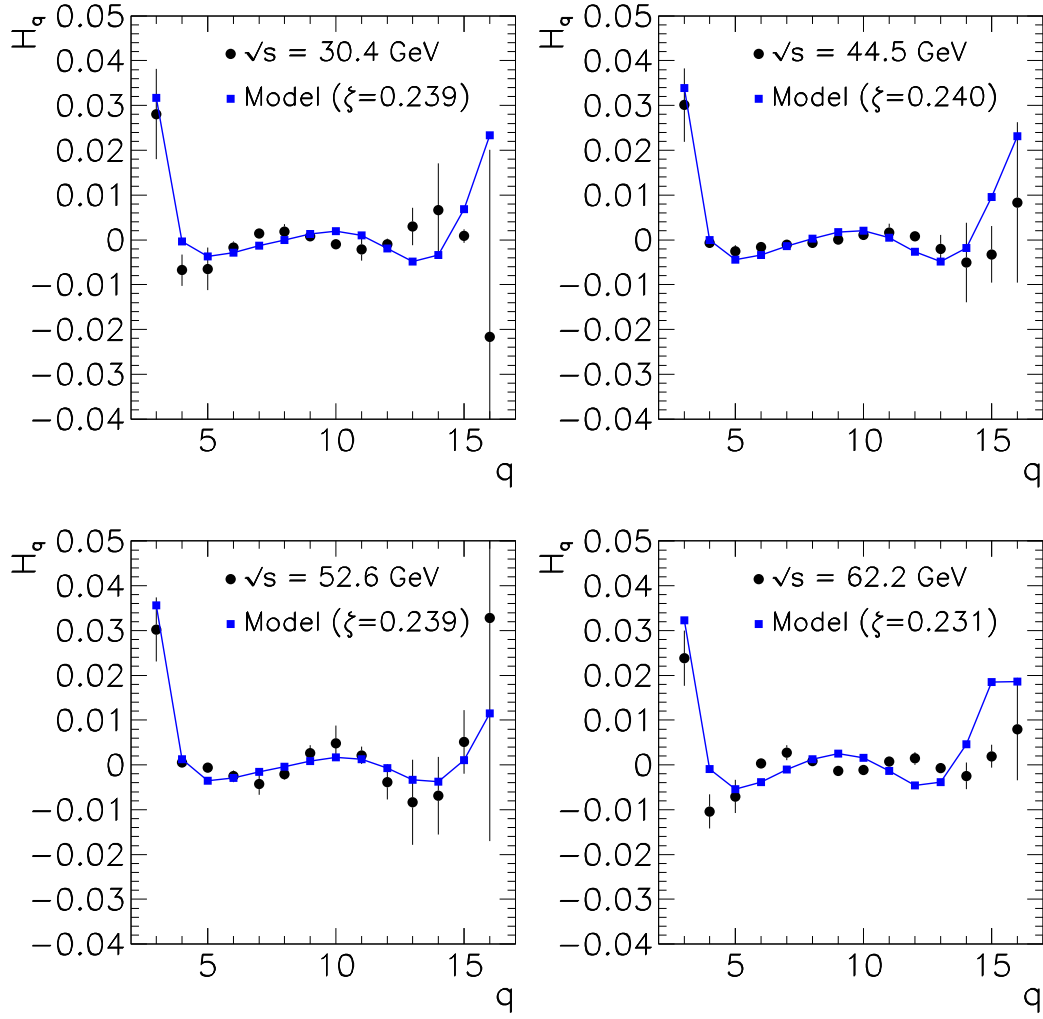


FIG. 6. Theoretical and experimental plots of H_q against q for pp at ISR energies.

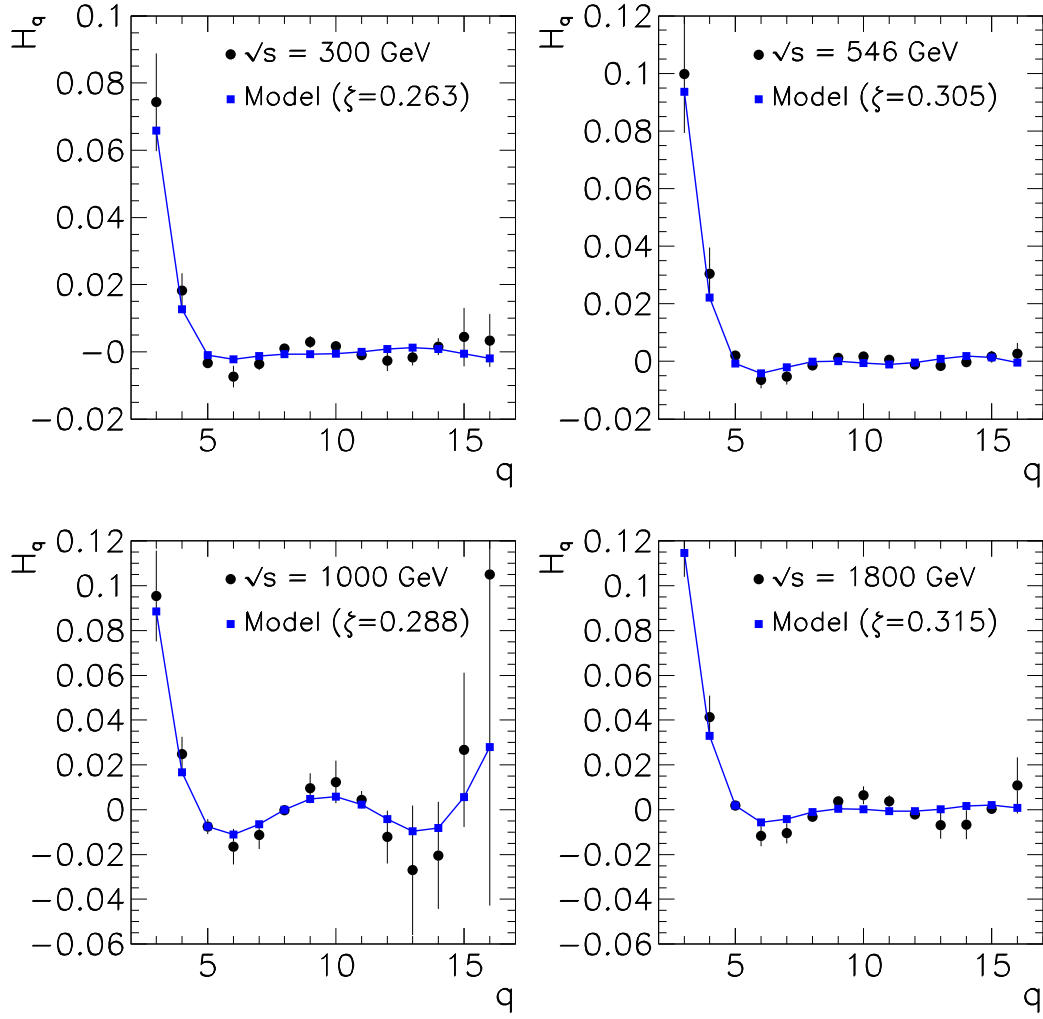


FIG. 7. Theoretical and experimental plots of H_q against q for $\bar{p}p$ at Collider energies.

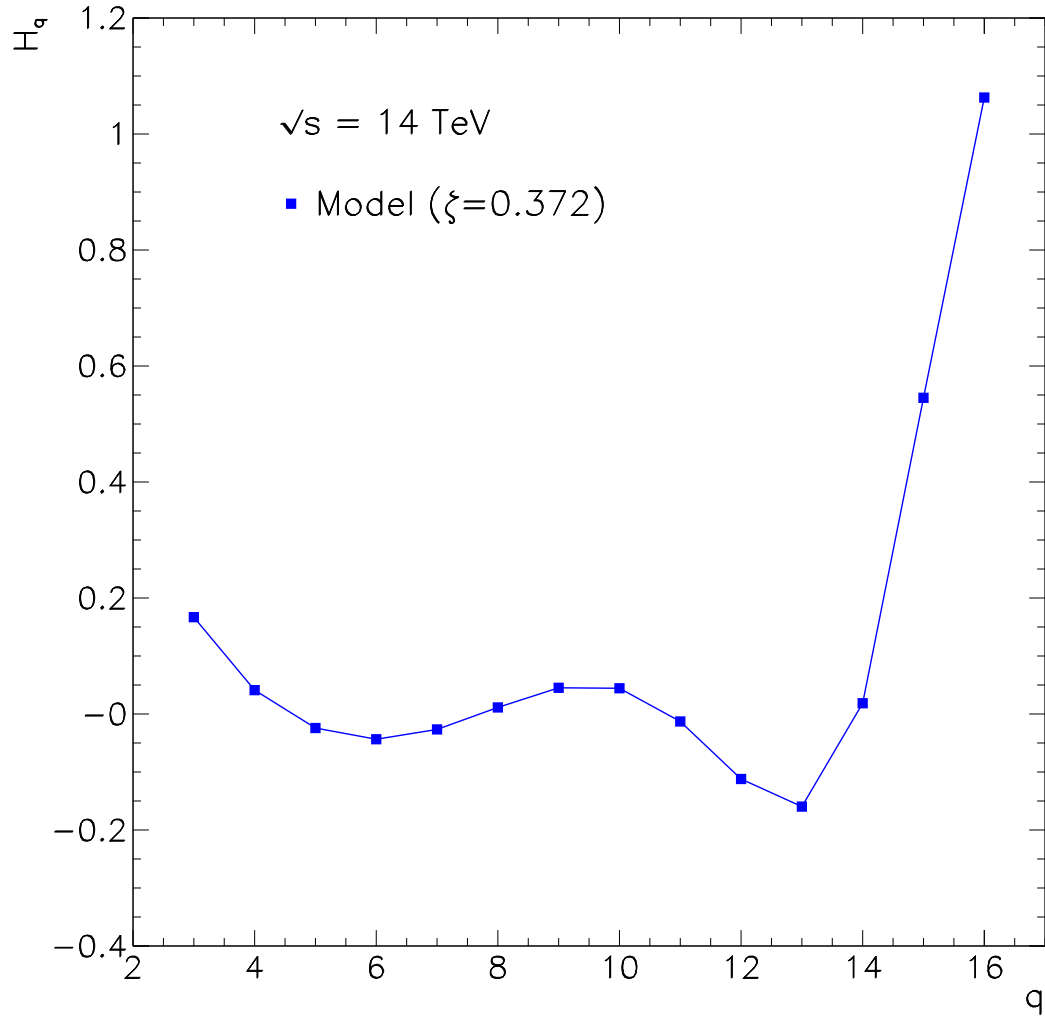


FIG. 8. Theoretical prediction for the ratio of the normalized factorial cumulant K_q to the factorial moment F_q at $\sqrt{s} = 14$ TeV.